

Surrogate-Based Bayesian Inverse Modeling of the Hydrological System: An Adaptive Approach Considering Surrogate Structural Error

Jiangjiang Zhang¹, Laosheng Wu², and Lingzao Zeng¹

¹ Zhejiang Provincial Key Laboratory of Agricultural Resources and Environment, Institute of Soil and Water Resources and Environmental Science, College of Environmental and Resource Sciences, Zhejiang University, Hangzhou, China,

² Department of Environmental Sciences, University of California, Riverside, CA, USA

Correspondence to:

L. Zeng,
lingzao@zju.edu.cn

Abstract

Inverse modeling is vital for an improved hydrological prediction. However, this process can be computationally demanding as it usually requires a large number of model evaluations. To address this issue, one can take advantage of surrogate modeling techniques, e.g., the one based on sparse polynomial chaos expansion (PCE). Nevertheless, when structural error of the surrogate model is neglected in inverse modeling, the inversion results will be biased. In this paper, we develop a surrogate-based Bayesian inversion framework that rigorously quantifies and gradually eliminates the structural error of the surrogate. Specifically, two strategies are proposed and compared. The first strategy works by obtaining an ensemble of sparse PCE surrogates with Markov chain Monte Carlo sampling, while the second one uses Gaussian process (GP) to simulate the structural error of a single sparse PCE surrogate. With an active learning process, the surrogate structural error can be gradually reduced to a negligible level in the posterior region, where the original input-output relationship can be much more easily captured by PCE than in the prior. Demonstrated by one numerical case of groundwater contaminant source identification with 28 unknown input variables, it is found that both strategies can efficiently reduce the bias introduced by surrogate modeling, while the second strategy has a better performance as it integrates two methods (i.e., PCE and GP) that complement each other.

1. Introduction

Uncertainty is ubiquitous in measuring, analyzing and predicting the system of concern in many different fields (Smith, 2014). In hydrological science, there is a growing interest in quantifying different sources of uncertainties with numerical modeling techniques, e.g., sensitivity analysis, failure probability analysis and data assimilation (Liu & Gupta, 2007; Song *et al.*, 2015; Tartakovsky, 2013; Vrugt *et al.*, 2008; Zhang *et al.*, 2017). To obtain an improved hydrological prediction, it is vital to reduce the uncertainty of model inputs (e.g., model parameters, initial conditions and boundary conditions) by conditioning on measurements of model outputs with inverse modeling methods (Osorio-Murillo *et al.*, 2015; Vrugt, 2016). Over the past decades, numerous inverse methods have been developed and/or applied in hydrological science, e.g., local and global optimization methods (Ahmad *et al.*, 2014; Duan *et al.*, 1992; Reed *et al.*, 2013), ensemble Kalman filter and its variants (Chen & Zhang, 2006; Emerick & Reynolds, 2013; Evensen, 2009; Song *et al.*, 2014; Zhang *et al.*, 2018b), particle filter (Moradkhani *et al.*, 2005; Vrugt *et al.*, 2013; Weerts & El Serafy, 2006), and Markov chain Monte Carlo (MCMC) (Smith & Marshall, 2008; Vrugt *et al.*, 2003; Vrugt *et al.*, 2008; Zhang *et al.*, 2015).

In this paper, our concern is MCMC, which is a commonly used method that can sample the posterior distribution of model inputs in a consistent and coherent manner (Brooks *et al.*, 2011; Vrugt, 2016). Over the past decade, MCMC has become increasingly popular in hydrological simulations (Cao *et al.*, 2018; Gaume *et al.*, 2010; Goharian *et al.*, 2018; Kuczera *et al.*, 2010; Vrugt & Beven, 2018). However, when

implementing MCMC for inverse modeling, a large number of model evaluations are usually required, especially for high-dimensional, strongly nonlinear problems. When the model is CPU-intensive (then we call it the high-fidelity model), the computational cost of MCMC simulation will be prohibitive.

To address this issue, one can take advantage of surrogate modeling techniques (*Asher et al.*, 2015; *Razavi et al.*, 2012). A surrogate model can be a data-driven model based on regression or interpolation, a reduced-order model obtained by projecting the original parameters and states onto their lower-dimensional subspace, or a numerical model with a reduced precision, etc. (*Smith*, 2014). Compared to the high-fidelity model, the surrogate model can obtain similar model outputs but at a much lower computational cost. Due to their efficiency, different forms of surrogate models have been applied in MCMC simulations of the hydrological system. For example, *Zeng et al.* (2012) used adaptive sparse grid interpolation, and *Laloy et al.* (2013) used generalized polynomial chaos expansion (PCE) to construct surrogates to accelerate posterior exploration of groundwater models, respectively. Inevitably, due to the existence of surrogate structural error (i.e., the difference between the high-fidelity and the surrogate model outputs), using surrogate models directly in MCMC simulations will introduce some bias. To correct this bias, *Zeng et al.* (2012) and *Laloy et al.* (2013) implemented two-stage MCMC simulations (i.e., sufficiently explored the parameter space with the surrogate model at stage one, then evaluated the high-fidelity model for correction at stage two) instead of the simple surrogate-based MCMC simulation. Another strategy to handle the surrogate structural error is to build a locally accurate

surrogate in the posterior region. To realize this idea, one can first identify the posterior region with an optimization method and then build the surrogate model and implement the surrogate-based MCMC simulation therein (*Zhang et al.*, 2013). This strategy can also be conveniently realized by an iterative process of surrogate-based MCMC simulation and surrogate refinement with accordingly added new training data (*Gong & Duan*, 2017; *Zhang et al.*, 2016). It is shown that this strategy can obtain satisfying inversion results with a small number of the high-fidelity model evaluations. Moreover, if this strategy is integrated with multi-fidelity simulation, an improved computational efficiency (i.e., fewer high-fidelity model evaluations) can be observed (*Zhang et al.*, 2018a).

Nevertheless, in the above approaches, structural error of the surrogate is not rigorously quantified. In this paper, we formulate an adaptive framework that rigorously quantifies and gradually eliminates the structural error of the surrogate. Here, we use the adaptive sparse PCE based on least angle regression (LARS) proposed by *Blatman & Sudret* (2011) to construct a surrogate for the high-fidelity model. To address “the curse of dimensionality”, i.e., the computational cost of surrogate construction grows rapidly with the dimension of model inputs (*Xiu*, 2010), LARS-PCE adaptively detects the important PCE terms with LARS and assigns zero-coefficients to the unimportant terms (which is called the sparse representation). Thus, in some practical applications, one can set high PCE degrees in nonlinear problems to obtain good performances without significantly increasing the computational cost of surrogate construction (*Blatman & Sudret*, 2010; 2011; *Elsheikh et al.*, 2014). In high-dimensional and

strongly nonlinear problems, however, the structural error of the LARS-PCE surrogate is still considerable. In this work, we will show that the surrogate structural error should not be neglected and a better performance can be achieved if this error is explicitly quantified and gradually reduced in an adaptive manner.

To quantify the structural error of the LARS-PCE surrogate, we propose and compare two strategies. In the first strategy, instead of using the single surrogate constructed by LARS-PCE, we further obtain an ensemble of PCE surrogates by drawing multiple realizations of the PCE coefficients with MCMC, conditioned on the same training data set used by LARS-PCE. Then we can obtain multiple sets of competing surrogate outputs, which can be used to assess the surrogate structural uncertainty. This strategy shares some similarity with the widely used method of Bayesian model averaging, which adopts multiple numerical models to represent conceptual model uncertainty (*Duan et al.*, 2007; *Madadgar & Moradkhani*, 2014; *Ye et al.*, 2010). This idea is also inspired by the work of (*Arnst et al.*, 2010), where the PCE coefficients are simulated as random variables in a Bayesian framework. In the second strategy, we directly simulate the surrogate structural error with a machine learning method, i.e., Gaussian process (GP) (*Rasmussen & Williams*, 2006), based on the difference between the high-fidelity and the LARS-PCE surrogate model outputs at the training points. Then we use the LARS-PCE outputs plus the GP outputs as the corrected surrogate outputs in MCMC simulations. In developing the second strategy, we have also drawn some inspiration from another way of treating conceptual model error, i.e., explicitly characterizing the difference between the actual measurement data

and the corresponding model outputs with a statistical method. e.g., GP (*Xu & Valocchi, 2015; Xu et al., 2017*).

Generally, the posterior distribution of model inputs occupies only a small proportion of the prior distribution. Thus, the variance of the high-fidelity model outputs in the posterior will be much smaller than that in the prior, which means the input-output relationship of the high-fidelity model can be much more accurately captured by LARS-PCE in the posterior than in the prior. With an active learning process proposed in our previous works (*Zhang et al., 2016; Zhang et al., 2018a*), we can gradually reduce the surrogate structural error to a negligible level in the posterior region. To our best knowledge, this adaptive approach to quantify and eliminate the surrogate structural error is rather new. And as will be demonstrated in the latter part of this paper, this adaptive approach can obtain both high efficiency and accuracy in MCMC simulations. Thus, we believe that the above approach has its value in both theoretical and practical aspects.

The remainder of this paper is structured as follows. In Section 2, we present some essential knowledge about MCMC, LARS-PCE, and the adaptive approach to quantify and eliminate the surrogate structural error. Then in Section 3, we demonstrate the performance of the proposed approach in one numerical case of groundwater contaminant source identification with 28 unknown input variables. Finally, some conclusions are provided in Section 4.

2. Methods

For simplicity, we can represent the hydrological model of concern in the

following form:

$$\tilde{\mathbf{y}} = f(\mathbf{m}) + \boldsymbol{\epsilon}, \quad (1)$$

where $f(\cdot)$ is the high-fidelity model with inputs $\mathbf{m} \in \mathbb{R}^{N_m \times 1}$, $\tilde{\mathbf{y}} \in \mathbb{R}^{N_y \times 1}$ is a vector for the measurements with error $\boldsymbol{\epsilon} \in \mathbb{R}^{N_y \times 1}$, respectively. Our initial knowledge about the model inputs \mathbf{m} is represented by a prior distribution $p(\mathbf{m})$. When the measurements $\tilde{\mathbf{y}}$ are available, we can update our knowledge about \mathbf{m} according to Bayes' theorem:

$$p(\mathbf{m}|\tilde{\mathbf{y}}) = \frac{p(\mathbf{m})p(\tilde{\mathbf{y}}|\mathbf{m})}{\int p(\tilde{\mathbf{y}}|\mathbf{m})p(\mathbf{m})d\mathbf{m}} \propto p(\mathbf{m})\mathcal{L}(\mathbf{m}|\tilde{\mathbf{y}}), \quad (2)$$

where $p(\mathbf{m}|\tilde{\mathbf{y}})$ is the posterior distribution, $\mathcal{L}(\mathbf{m}|\tilde{\mathbf{y}}) \equiv p(\tilde{\mathbf{y}}|\mathbf{m})$ is the likelihood, and $p(\tilde{\mathbf{y}}) = \int p(\tilde{\mathbf{y}}|\mathbf{m})p(\mathbf{m})d\mathbf{m}$ is the so-called Bayesian evidence or marginal likelihood, which is a constant. When the measurement error $\boldsymbol{\epsilon}$ is normally distributed with zero-mean and covariance $\boldsymbol{\Sigma} \in \mathbb{R}^{N_y \times N_y}$, the likelihood can be expressed as:

$$\mathcal{L}(\mathbf{m}|\tilde{\mathbf{y}}) = \frac{1}{(2\pi)^{N_y/2}|\boldsymbol{\Sigma}|^{1/2}} \exp\left\{-\frac{1}{2}[\tilde{\mathbf{y}} - f(\mathbf{m})]^T \boldsymbol{\Sigma}^{-1} [\tilde{\mathbf{y}} - f(\mathbf{m})]\right\}, \quad (3)$$

where $|\cdot|$ is the determinant operator, and the superscript T means transpose operation. In nonlinear, complex problems, $p(\mathbf{m}|\tilde{\mathbf{y}})$ usually cannot be obtained analytically. Then one has to approximate the posterior with a numerical method, e.g., MCMC.

2.1. Markov Chain Monte Carlo (MCMC)

MCMC works by generating a (quasi-)random walk through the parameter space to from one or more Markov chains. Under strict conditions of ergodicity and reversibility, the chain(s) can converge to the target distribution, i.e., the posterior

distribution of model inputs in this paper, after enough steps (i.e., the so-called burn-in period). Then one can use samples in the chains to approximate the statistics of $p(\mathbf{m}|\tilde{\mathbf{y}})$.

MCMC can be implemented with the following procedure (*Brooks et al.*, 2011):

Step 1. At the initial step, draw an initial state \mathbf{m}_0 of the Markov chain(s) from the prior distribution, i.e., $\mathbf{m}_0 \sim p(\mathbf{m})$.

Step 2. At step t ($t \geq 1$), generate a proposal state \mathbf{m}_p from a proposal distribution $q(\cdot)$ conditioned on the previous state \mathbf{m}_{t-1} , i.e., $\mathbf{m}_p \sim q(\mathbf{m}_p|\mathbf{m}_{t-1})$.

Step 3. According to the Metropolis-Hastings rule (*Hastings*, 1970; *Metropolis et al.*, 1953), accept \mathbf{m}_p with the following probability:

$$p_{\text{acc}} = \min \left\{ 1, \frac{p(\mathbf{m}_p|\tilde{\mathbf{y}})q(\mathbf{m}_{t-1}|\mathbf{m}_p)}{p(\mathbf{m}_{t-1}|\tilde{\mathbf{y}})q(\mathbf{m}_p|\mathbf{m}_{t-1})} \right\}, \quad (4)$$

where $p(\mathbf{m}_p|\tilde{\mathbf{y}})$ and $p(\mathbf{m}_{t-1}|\tilde{\mathbf{y}})$ are the posterior densities of \mathbf{m}_p and \mathbf{m}_{t-1} , $q(\mathbf{m}_{t-1}|\mathbf{m}_p)$ and $q(\mathbf{m}_p|\mathbf{m}_{t-1})$ are the probabilities of trail moves from \mathbf{m}_p to \mathbf{m}_{t-1} and from \mathbf{m}_{t-1} to \mathbf{m}_p , respectively.

Step 4. Let $t = t + 1$, repeat Steps 2-3 until $t = t_{\text{max}}$ (i.e., the user-defined maximum iteration number).

Over the past decade, many algorithms have been developed to improve the efficiency of MCMC simulations. In this paper, we adopt the DREAM_(ZS) algorithm that uses a mixture of parallel and snooker jumping distributions to generate the proposal states based on a thinned history of the Markov chains. For the implementation details of DREAM_(ZS), one can refer to (*Laloy & Vrugt*, 2012; *Laloy et al.*, 2013; *Vrugt*, 2016).

2.2. Surrogate Construction with LARS-PCE

Generally, MCMC requires a large number of iterations to reach convergence, which means a high computational cost when the hydrological model $f(\mathbf{m})$ is CPU-intensive. In this situation, using a CPU-efficient surrogate $\hat{f}(\mathbf{m})$ in the MCMC simulation will be an appropriate option. Here, we use the LARS-PCE method proposed by *Blatman & Sudret* (2011) to construct a surrogate for the high-fidelity model.

In PCE, the model output is approximated with orthogonal polynomials in the follows way:

$$f(\mathbf{m}) \approx \hat{f}(\mathbf{m}) = \sum_{i=0}^{P-1} c_i \psi_i(\mathbf{m}) = \mathbf{c}^T \boldsymbol{\Psi}(\mathbf{m}), \quad (5)$$

where $\boldsymbol{\Psi}(\mathbf{m}) = \{\psi_0(\mathbf{m}), \dots, \psi_{P-1}(\mathbf{m})\}^T$ are orthogonal polynomials over the model input distribution, $\mathbf{c} = \{c_0, \dots, c_{P-1}\}^T$ are the corresponding coefficients that can be determined with the intrusive Galerkin method, or the non-intrusive projection/regression methods (*Choi et al.*, 2004; *Xiu*, 2010), and P is the total number of PCE terms, respectively. Here, “orthogonal” means that

$$\langle \psi_i(\mathbf{m}), \psi_j(\mathbf{m}) \rangle = \int_{\Theta} \psi_i(\mathbf{m}) \psi_j(\mathbf{m}) p(\mathbf{m}) d\mathbf{m} = \begin{cases} 0 & \text{if } i \neq j, \\ 1 & \text{if } i = j, \end{cases} \quad (6)$$

where Θ is the support of $p(\mathbf{m})$.

As the number of $f(\mathbf{m})$ evaluations needed by surrogate construction increases with the number of PCE terms (which grows dramatically with the input dimension), it is beneficial to only retain the terms that have significant impacts on the model output and set zero-coefficients to the other unimportant terms. This turns the classical “full” PCE to a sparse PCE (*Blatman & Sudret*, 2008). In LARS-PCE, a hyperbolic scheme

is used to truncate the PCE terms for a sparse representation, which favors the low-order interactions more than the high-order interactions in the model. The significant PCE coefficients are automatically detected by least angle regression (*Efron et al.*, 2004) in an adaptive manner. To check the accuracy of the sparse PCE surrogate, the corrected leave-one-out error can be calculated for assessment. Then the obtained sparse PCE can be represented as:

$$f(\mathbf{m}) \approx \hat{f}(\mathbf{m}) = \sum_{j=0}^{Q-1} c_j^s \psi_j^s(\mathbf{m}) = \mathbf{c}^s \mathbf{\Psi}^s(\mathbf{m}), \quad (7)$$

where $\mathbf{\Psi}^s(\mathbf{m}) = \{\psi_0^s(\mathbf{m}), \dots, \psi_{Q-1}^s(\mathbf{m})\}^T$ are the significant orthogonal polynomials, $\mathbf{c}^s = \{c_0^s, \dots, c_{Q-1}^s\}^T$ are the corresponding coefficients, and Q is the total number of PCE terms that are retained.

In LARS-PCE, one can set high PCE degrees in nonlinear problems to obtain good performances without significantly increasing the computational cost of surrogate construction (i.e., the number of $f(\mathbf{m})$ evaluations). As the LARS-PCE method itself is not the focus of this paper, further details about this method are not presented here. Interested readers can refer to (*Blatman & Sudret*, 2011). Moreover, a MATLAB package named UQLab that includes LARS-PCE and many other useful algorithms for uncertainty quantification is also available (*Marelli & Sudret*, 2014).

2.3. The Adaptive Approach to Quantify and Eliminate the Surrogate Structural Error

Then we can use the surrogate $\hat{f}(\mathbf{m})$ constructed by LARS-PCE in MCMC simulation to gain efficiency. Nevertheless, due to the unavoidable discrepancy

between the high-fidelity and the surrogate model outs, using $\hat{f}(\mathbf{m})$ directly in MCMC simulation will introduce some bias. Below we will propose two strategies to quantify the surrogate structural error and an adaptive approach to gradually eliminate this error in the posterior region.

2.3.1. Strategy A

The idea behind the first strategy (Strategy A) is that using a single PCE surrogate can overlook the surrogate structural uncertainty, and it will be better to obtain an ensemble of competing surrogates. In LARS-PCE, as the significant PCE terms (i.e., the significant orthogonal polynomials Ψ^s) have been identified, we can assess the surrogate structural uncertainty through evaluating the uncertainty of the PCE coefficients \mathbf{c}^s . To realize this idea, we can treat \mathbf{c}^s as uncertain variables and use MCMC to sample the posterior distribution of \mathbf{c}^s , conditioned on the high-fidelity training data used to construct the LARS-PCE surrogate.

Here, we set the coefficients obtained by LARS-PCE as the initial state of MCMC, which is beneficial for a quick convergence. The Gaussian likelihood with measurement error integrated out is used to evaluate the performance of each state in the Markov chains (Vrugt, 2016). For the sake of numerical stability, we will use the log-likelihood instead of the likelihood in the MCMC simulation, i.e.,

$$\mathcal{L}_{\log}(\mathbf{c}^s | \mathbf{Y}) = -\frac{N_t}{2} \log \left\{ \sum_{i=1}^{N_t} [\mathbf{c}^{sT} \Psi^s(\mathbf{m}_i) - f(\mathbf{m}_i)]^2 \right\}, \quad (8)$$

where $\mathbf{M} = \{\mathbf{m}_1, \dots, \mathbf{m}_{N_t}\}$ and $\mathbf{Y} = \{f(\mathbf{m}_1), \dots, f(\mathbf{m}_{N_t})\}$ are the high-fidelity training data, and N_t is the number of training data points. Finally, we can obtain an

ensemble of N_e posterior samples of \mathbf{c}^s , i.e., $\{\mathbf{c}_1^s, \dots, \mathbf{c}_{N_e}^s\}$. Given an arbitrary set of model inputs \mathbf{m}^* , we can thus obtain an ensemble of surrogate outputs, i.e., $\hat{\mathbf{F}} = \{\mathbf{c}_1^{s^T} \boldsymbol{\Psi}^s(\mathbf{m}^*), \dots, \mathbf{c}_{N_e}^{s^T} \boldsymbol{\Psi}^s(\mathbf{m}^*)\}$, to explicitly represent the surrogate structural uncertainty.

2.3.2. Strategy B

In the second strategy (Strategy B), we will use a machine learning method, i.e., Gaussian process (GP), to directly simulate the surrogate structural error, i.e., $g(\mathbf{m}) = f(\mathbf{m}) - \hat{f}(\mathbf{m})$. GP uses a (multivariate) Gaussian distribution to predict the quantity of interest (QoI):

$$\text{QoI} \sim \mathcal{GP}(\mu(\cdot), k(\cdot, \cdot)), \quad (9)$$

where $\mu(\cdot)$ is the mean function, and $k(\cdot, \cdot)$ is the covariance function. In this paper, the most common zero-mean prior function $\mu(\mathbf{m}) = 0$ and squared exponential covariance function

$$k(\mathbf{m}, \mathbf{m}') = \sigma^2 \exp \left[-\frac{1}{2} \sum_{n=1}^{N_m} \left(\frac{\mathbf{m}_n - \mathbf{m}'_n}{l_n} \right)^2 \right] \quad (10)$$

are used (Rasmussen & Williams, 2006). Here σ and $\{l_1, \dots, l_{N_m}\}$ are hyperparameters of the covariance function, \mathbf{m} and \mathbf{m}' are two arbitrary sets of model inputs, respectively.

Based on the training data $\mathbf{M} = \{\mathbf{m}_1, \dots, \mathbf{m}_{N_t}\}$ and $\mathbf{E} = \{g(\mathbf{m}_1), \dots, g(\mathbf{m}_{N_t})\}$, we can train the GP system and obtain the conditional mean and variance of the QoI at an arbitrary set of model inputs \mathbf{m}^* :

$$\mu_{|\mathbf{E}}(\mathbf{m}^*) = k(\mathbf{m}^*, \mathbf{M}) k^{-1}(\mathbf{M}, \mathbf{M}) \mathbf{E}, \quad (11)$$

$$\sigma^2|_{\mathbf{E}} = k(\mathbf{m}^*, \mathbf{m}^*) - k(\mathbf{m}^*, \mathbf{M})k^{-1}(\mathbf{M}, \mathbf{M})k(\mathbf{M}, \mathbf{m}^*), \quad (12)$$

where the i th component of $k(\mathbf{m}^*, \mathbf{M}) \in \mathbb{R}^{1 \times N_t}$ is $k(\mathbf{m}^*, \mathbf{m}_i)$, the component at the i th row and j th column of $k(\mathbf{M}, \mathbf{M}) \in \mathbb{R}^{N_t \times N_t}$ is $k(\mathbf{m}_i, \mathbf{m}_j)$, and $k(\mathbf{M}, \mathbf{m}^*) \in \mathbb{R}^{N_t \times 1}$ is the transpose of $k(\mathbf{m}^*, \mathbf{M})$, respectively.

Then we can use the conditional mean function defined in equation (11) to approximate the surrogate structural error $g(\mathbf{m})$, i.e., $g(\mathbf{m}) \approx \mu_{|\mathbf{E}}(\mathbf{m})$. In MCMC simulation, we will use $\hat{f}_c(\mathbf{m}) = \hat{f}(\mathbf{m}) + \mu_{|\mathbf{E}}(\mathbf{m})$ as the corrected surrogate output to account for the surrogate structural error.

2.3.3. The Adaptive Process to Eliminate the Surrogate Structural Error

Nevertheless, in many nonlinear hydrological systems, given a limited (and even a rather large) number of high-fidelity training data drawn from the prior distribution, the original input-output relationship generally cannot be accurately captured even by a state-of-the-art surrogate modeling technique, e.g., LARS-PCE. On the other hand, as the posterior usually occupies a small proportion of the prior distribution, the variance of the high-fidelity model outputs in the posterior will be much smaller than that in the prior, which means the input-output relationship of the high-fidelity model can be much more easily captured by the surrogate in the posterior. Based on this idea, here we formulate an active learning process that iteratively adds new training data that gradually approach to the posterior region to refine the surrogate locally. At each iteration, the added training data are sampled from the approximated posterior of a surrogate-based MCMC simulation. After enough iterations, we can obtain a locally accurate surrogate and an accurate estimation of the posterior distribution.

A complete procedure of the approach proposed in this paper is given in Algorithm 1. At the beginning, N_t random samples are drawn from the prior distribution of model inputs, i.e., $\mathbf{M} = \{\mathbf{m}_1, \dots, \mathbf{m}_{N_t}\}$. With \mathbf{M} and the corresponding model outputs $\mathbf{Y} = \{f(\mathbf{m}_1), \dots, f(\mathbf{m}_{N_t})\}$, we can train and obtain an initial surrogate $\hat{f}_0(\mathbf{m})$ using the LARS-PCE method. Generally, the accuracy of $\hat{f}_0(\mathbf{m})$ is far from enough to obtain satisfying inversion results in MCMC simulation where Strategy A or Strategy B is used to account for the structural error of $\hat{f}_0(\mathbf{m})$. Nevertheless, the approximated posterior $\tilde{p}_0(\mathbf{m}|\tilde{\mathbf{y}})$ is slightly closer to the real posterior than the prior $p(\mathbf{m})$. From $\tilde{p}_0(\mathbf{m}|\tilde{\mathbf{y}})$, we can draw N_a samples $\mathbf{M}_a = \{\mathbf{m}_{a,1}, \dots, \mathbf{m}_{a,N_a}\}$ that are closer to the posterior than the prior samples. Then we can add them to the pool of existing training data set, i.e., $\mathbf{M} = \{\mathbf{M}, \mathbf{M}_a\}$ and $\mathbf{Y} = \{\mathbf{Y}, \mathbf{Y}_a\}$, where \mathbf{Y}_a are the high-fidelity model outputs of \mathbf{M}_a , and construct a new surrogate $\hat{f}_1(\mathbf{m})$ accordingly. In constructing the surrogate, the computational time increases with the number of training data points. So in practice we can also use a subset of $\{\mathbf{M} \mathbf{Y}\}$, where the samples that are far from the measurements $\tilde{\mathbf{y}}$ are discarded (e.g., using the likelihood function defined in equation (3) as a measure). To improve the efficiency of MCMC simulation, we will use a thinned chain history of the previous MCMC simulation to generate the initial states for the present MCMC simulation. In this way, the present MCMC simulation is actually connected with the previous one and thus it can converge to the stationary regime very quickly. The aforementioned surrogate refinement and surrogate-based MCMC simulation that considers surrogate structural error will be further iterated $I_{\max} - 1$ times. Finally, the posterior is approximated with $\tilde{p}_{I_{\max}}(\mathbf{m}|\tilde{\mathbf{y}})$.

Algorithm 1 Adaptive surrogate-based MCMC simulation considering surrogate structural error.

1. Draw N_t random samples from $p(\mathbf{m})$, i.e., $\mathbf{M} = \{\mathbf{m}_1, \dots, \mathbf{m}_{N_t}\}$, calculate $\mathbf{Y} = \{f(\mathbf{m}_1), \dots, f(\mathbf{m}_{N_t})\}$.
2. Build an initial LARS-PCE surrogate $\hat{f}_0(\mathbf{m})$ based on $\{\mathbf{M} \mathbf{Y}\}$.
3. Run MCMC with $\hat{f}_0(\mathbf{m})$ and Strategy A or B, obtain $\tilde{p}_0(\mathbf{m}|\tilde{\mathbf{y}})$.
4. **for** $i = 1, \dots, I_{\max}$ **do**
 Draw N_a random samples, $\mathbf{M}_a = \{\mathbf{m}_{a,1}, \dots, \mathbf{m}_{a,N_a}\}$, from $\tilde{p}_{i-1}(\mathbf{m}|\tilde{\mathbf{y}})$, calculate $\mathbf{Y}_a = \{f(\mathbf{m}_{a,1}), \dots, f(\mathbf{m}_{a,N_a})\}$. Let $\mathbf{M} = \{\mathbf{M}, \mathbf{M}_a\}$, $\mathbf{Y} = \{\mathbf{Y}, \mathbf{Y}_a\}$.
 Build a LARS-PCE surrogate $\hat{f}_i(\mathbf{m})$ based on $\{\mathbf{M} \mathbf{Y}\}$ or their subset.
 Based on previous MCMC simulation results, run MCMC with $\hat{f}_i(\mathbf{m})$ and Strategy A or B, obtain $\tilde{p}_i(\mathbf{m}|\tilde{\mathbf{y}})$.
end for
5. The posterior is approximated with $\tilde{p}_{I_{\max}}(\mathbf{m}|\tilde{\mathbf{y}})$.

3. Illustrative Example

To demonstrate the performance of the proposed method, we will test in this section a numerical case that solves a groundwater contaminant source identification problem, which is adopted from our previous study (*Zhang et al.*, 2018a). This case study involves nonlinear processes that have 28 unknown model input variables, which poses a challenge for solving an inverse problem.

[Figure 1]

Here, we consider steady-state saturated groundwater flow and solute transport in a confined aquifer. In the horizontal direction, the length of the domain is 20[L], and in the vertical direction, the length is 10[L] (Figure 1). On the upper and lower sides of the domain, the no-flow condition is prescribed. While on the left and right sides, the constant-head condition is prescribed (12[L] and 11[L], respectively). At the initial time, the hydraulic head is 11[L] everywhere except for the left boundary (12[L]). With the above initial conditions and boundary conditions, we can obtain a steady-state

flow field by solving

$$\frac{\partial}{\partial x_i} \left(K_i \frac{\partial h}{\partial x_i} \right) = 0 \quad (13)$$

and

$$v_i = -\frac{K_i}{\theta} \frac{\partial h}{\partial x_i} \quad (14)$$

numerically with MODFLOW (*Harbaugh et al.*, 2000). Here $x_i[\text{L}]$ signifies the distance in the respective direction ($i = 1$ for the x direction and $i = 2$ for the y direction), $h[\text{L}]$ is the hydraulic head, $K_i[\text{LT}^{-1}]$ represents the component of hydraulic conductivity in the i th direction, $\theta[-]$ is the porosity of the aquifer, and $v_i[\text{LT}^{-1}]$ denotes the velocity of pore water in the i th direction, respectively. Here the conductivity field is unknown and heterogeneous, whose log-transformed values $Y = \ln K$ are spatially correlated according to the following function:

$$C_Y(x_a, y_a; x_b, y_b) = \sigma_Y^2 \exp \left(-\frac{|x_a - x_b|}{l_x} - \frac{|y_a - y_b|}{l_y} \right), \quad (15)$$

where (x_a, y_a) and (x_b, y_b) are two arbitrary locations, σ_Y^2 signifies the variance of the Y field, and $l_x(l_y)$ denotes the correlation length in the $x(y)$ direction, respectively. Utilizing this correlation relationship, we can reduce the dimensionality of the Y field with the Karhunen-Loeve (KL) expansion (*Zhang & Lu*, 2004) from the model grid number (81×41) to the number of truncated KL terms (N_{KL}):

$$Y(\mathbf{x}) \approx \bar{Y}(\mathbf{x}) + \sum_{i=1}^{N_{\text{KL}}} \sqrt{\tau_i} s_i(\mathbf{x}) \xi_i, \quad (16)$$

where $\mathbf{x} = (x, y)$ signifies the location, $\bar{Y}(\mathbf{x})$ is the mean function of the Y field, $s_i(\mathbf{x})$ and τ_i denote the eigenfunctions and eigenvalues of the correlation function of

equation (15), and ξ_i represent independent standard Gaussian random variables, respectively. Here, we retain $N_{\text{KL}} = 20$ KL terms, which can keep about 88.3% of the total variance of the Y field. In the flow process, the uncertainty only stems from the conductivity field, which is characterized by the 20 unknown KL terms. While other parameters are assumed to be known from field survey, i.e., $\theta = 0.25[-]$, $\sigma_Y^2 = 0.4$, $l_x = 10[\text{L}]$, $l_y = 5[\text{L}]$, and $\bar{Y}(\mathbf{x}) = 2$, respectively.

In the flow field, some amount of non-reactive solute is released from an unknown contaminant source that is located somewhere in the red dashed rectangle depicted in Figure 1. The strength of the source measured by the mass loading rate varies with time and is characterized by six parameters, i.e., $s_i[\text{MT}^{-1}]$ during $i \sim i + 1[\text{T}]$, for $i = 1, \dots, 6$. Then the contaminant concentration $C[\text{ML}^{-3}]$ at any time and location can be obtained by solving the advection-dispersion equation

$$\frac{\partial(\theta C)}{\partial t} = \frac{\partial}{\partial x_i} \left(\theta D_{ij} \frac{\partial C}{\partial x_j} \right) - \frac{\partial}{\partial x_i} (\theta v_i C) + q_s C_s \quad (17)$$

with MT3DMS (Zheng & Wang, 1999). Here, $t[\text{T}]$ is the time, $q_s[\text{T}^{-1}]$ is the volumetric flow rate per unit volume of the aquifer, $C_s[\text{ML}^{-3}]$ is the concentration of the contaminant source, and $D_{ij}[\text{L}^2\text{T}^{-1}]$ are the hydrodynamic dispersion coefficient tensors that have the following four components:

$$\begin{cases} D_{xx} = \frac{1}{\|\mathbf{v}\|^2} (\alpha_L v_x^2 + \alpha_T v_y^2), \\ D_{yy} = \frac{1}{\|\mathbf{v}\|^2} (\alpha_L v_y^2 + \alpha_T v_x^2), \\ D_{xy} = D_{yx} = \frac{1}{\|\mathbf{v}\|^2} (\alpha_L - \alpha_T) v_x v_y, \end{cases} \quad (18)$$

where α_L and $\alpha_T[\text{L}]$ signify the longitudinal and transverse dispersivities, and

$\|\mathbf{v}\|^2 = \sqrt{v_x^2 + v_y^2}$ denotes the magnitude of the velocity \mathbf{v} , respectively. In the solute transport process, the unknown parameters are the location of the contaminant source, i.e., $(x_s, y_s)[\text{L}]$, and the six source strength parameters, i.e., $s_1 \sim s_6[\text{MT}^{-1}]$. While other parameters are assumed to be known as $\alpha_L = 0.3[\text{L}]$ and $\alpha_T = 0.03[\text{L}]$, respectively.

So in total there are 28 unknown parameters, i.e., the 20 KL terms for the conductivity field and the eight source parameters. To infer the unknown parameters, we collect measurements of the head and concentration at the 15 wells denoted by the blue circles in Figure 1. As the flow field is steady-state, the head measurements are collected only once. Thus, there are 15 head measurements in total. The concentration measurements are obtained at five moments of $t = 6, 8, 10, 12, 14[\text{T}]$. Thus, there are 75 concentration measurements altogether. Here, the measurements are generated from one set of true model parameters \mathbf{m}_{true} with additive errors. In this case study, the measurement error of head is assumed to fit $\varepsilon_h \sim \mathcal{N}(0, 0.01^2)$, and for concentration measurement the error fits $\varepsilon_C \sim \mathcal{N}(0, 0.01^2)$. As mentioned above, the prior distribution for each component of the 20 KL terms is a standard Gaussian distribution, i.e., $\xi_i \sim \mathcal{N}(0, 1^2)$, for $i = 1, \dots, 20$. The prior distributions for the eight source parameters are all uniform. The corresponding ranges and true values of the source parameters are listed in Table 1.

[Table 1]

Based on the 90 measurements, we implement four different MCMC approaches to infer the unknown parameters. The four approaches are (1) the high-fidelity MCMC

simulation (Reference results), (2) the adaptive surrogate-based MCMC simulation without considering the surrogate structural error ($\hat{f}(\mathbf{m})$ -MCMC), (3) the adaptive surrogate-based MCMC simulation that considers the surrogate structural error with Strategy A ($\hat{f}(\mathbf{m})$ -MCMC+Strategy A), and (4) the adaptive surrogate-based MCMC simulation that considers the surrogate structural error with Strategy B ($\hat{f}(\mathbf{m})$ -MCMC+Strategy B), respectively.

[Figure 2]

In the high-fidelity MCMC simulation, there are 20 parallel chains. The length of each chain is 12,000, which means that the total number of the high-fidelity model evaluations is 240,000. The Gaussian likelihood defined in equation (3) is used to evaluate the goodness-of-fit between the measurements $\tilde{\mathbf{y}}$ and the corresponding model outputs $f(\mathbf{m})$. As shown in Figure 2, the chains (blue dots) for the eight source parameters can catch the true values (black crosses) after about 120,000 $f(\mathbf{m})$ evaluations. From the trace plots of the Markov chains, we can declare a good convergence for the high-fidelity MCMC simulation. Then we use the high-fidelity MCMC simulation results as a reference to check the performances of the three adaptive surrogate-based MCMC simulations.

The $\hat{f}(\mathbf{m})$ -MCMC simulation is implemented in the same way as Algorithm 1, except that neither Strategy A nor Strategy B is utilized to quantify the surrogate structural error. While $\hat{f}(\mathbf{m})$ -MCMC+Strategy A and $\hat{f}(\mathbf{m})$ -MCMC+Strategy B utilize Strategy A and Strategy B respectively to account for the surrogate structural error in a quantitative manner. When implementing Strategy A, we first calculate the

surrogate mean (μ_{PCE}) and covariance (Σ_{PCE}) from an ensemble of $N_e = 20$ competing surrogates. Then we use μ_{PCE} as the surrogate outputs and augment Σ_{PCE} to the measurement error covariance Σ in the likelihood function defined in equation (3). Under this Gaussian assumption for the surrogate structural error, Strategy A becomes similar to GP that uses a (multivariate) Gaussian distribution to approximate the model outputs. Nevertheless, we can also use a more sophisticated implementation of Strategy A, e.g., considering a non-Gaussian distribution for the surrogate structural error and adopting a more generalized likelihood function such as the one proposed by *Schoups & Vrugt (2010)*.

[Figure 3]

In the three adaptive surrogate-based MCMC simulations, the initial numbers of training data drawn from the prior distribution are all $N_t = 200$. Based on these initial training data, we can construct a LARS-PCE surrogate to accelerate the MCMC simulations. When implementing the surrogate-based MCMC algorithms, we again set the number of parallel chains as $N_c = 20$. At each iteration, we draw N_a random samples from the approximated posterior distribution as the new training data set \mathbf{M}_a . For the sake of convenience, we directly use the last samples at the N_c Markov chains, which can be viewed as N_c random samples drawn from the approximated posterior distribution. In practice, there would always exist some outlier chains in the surrogate-based MCMC simulations, especially at the early iterations. To address this issue, we will discard five of the N_c samples that have the worst performances according to the likelihood function, i.e., we will actually add $N_a = 15$ new training data at each

iteration. The coupled processes of surrogate refinement and surrogate-based MCMC simulation are iterated $I_{\max} = 25$ times. So in all the three adaptive surrogate-based MCMC simulations, the total numbers of the high-fidelity model evaluations are $N_{\text{ini}} + N_{\text{c}} * I_{\max} = 700$.

[Figure 4]

In Figure 2, we also show the posterior mean estimates of the eight source parameters obtained from $\hat{f}(\mathbf{m})$ -MCMC (red circles), $\hat{f}(\mathbf{m})$ -MCMC+Strategy A (red diamonds), and $\hat{f}(\mathbf{m})$ -MCMC+Strategy B (red squares), respectively. From this figure, we can find that if the surrogate structural error is not considered, the inversion results will be significantly biased, even though the adaptive process of surrogate refinement is implemented. In Figure 3, we plot the initial and added training data for the eight source parameters in the $\hat{f}(\mathbf{m})$ -MCMC approach. It again shows that neglecting the surrogate structural error will deteriorate the active learning process that is essential to obtain a locally accurate surrogate.

[Figure 5]

When the surrogate structural error is quantified with Strategy A or Strategy B, the posterior mean estimates of the eight source parameters can be greatly improved, while no extra high-fidelity model evaluations are required. In Figure 4 and Figure 5, we also plot the initial and added training data for the eight source parameters in the $\hat{f}(\mathbf{m})$ -MCMC+Strategy A and $\hat{f}(\mathbf{m})$ -MCMC+Strategy B approaches, respectively. From Figures 2~5, we can find that accounting for the surrogate structural error can significantly reduce the bias in the inversion results, while adopting Strategy B can

produce more accurate results than Strategy A. We think the reasons are twofold. First, in Strategy A, we are trying to add some uncertainty to the surrogate outputs so that they are more likely to cover the high-fidelity outputs. Although Strategy A can reduce the bias introduced by the surrogate structural error (this can be concluded by comparing Figure 3 and Figure 4), the approximated posterior distribution will be always wider due to the added surrogate uncertainty. Thus, Strategy A is still not an optimal choice although it is better than the $\hat{f}(\mathbf{m})$ -MCMC approach. Second, in Strategy B, we are trying to generate a direct jump from the surrogate outputs to the high-fidelity outputs, which introduces far less uncertainty than Strategy A. This can also be verified by comparing Figure 4 and Figure 5, where the training data generated by Strategy B are more concentrated. Moreover, as a regression-based method, LARS-PCE is better at simulating the global behavior of the high-fidelity model. While as a kernel-based method, GP is more skilled in capturing the local variations (e.g., the surrogate structural error). So we think one key factor of Strategy B is that it integrates two methods (i.e., LARS-PCE and GP) that complement each other. According to the above comparison and reasoning, the $\hat{f}(\mathbf{m})$ -MCMC+Strategy B approach is more recommended. In Figure 6, we further show the evolution of the error of the LARS-PCE surrogate at the true model parameters \mathbf{m}_{true} with the following indicator:

$$\text{Err}(i) = \sqrt{\sum_{j=1}^{N_y} \left[\frac{f_j(\mathbf{m}_{\text{true}}) - \hat{f}_{i,j}(\mathbf{m}_{\text{true}})}{\varepsilon_j} \right]^2}, \quad (19)$$

where i is the iteration index, ε_j is the standard deviation of the j th measurement, $\hat{f}_{i,j}(\mathbf{m}_{\text{true}})$ and $f_j(\mathbf{m}_{\text{true}})$ are the j th surrogate output constructed at the i th

iteration and the j th high-fidelity output, respectively. It is clear that using the recommended approach, we can gradually build a very accurate surrogate near the true model parameters.

[Figure 6]

4. Conclusions

In this paper, we propose an adaptive approach that rigorously quantifies and gradually eliminates the surrogate structural error in surrogate-based MCMC simulations. Here, two strategies are proposed to quantify the surrogate structural error. In the first strategy (Strategy A), we try to quantify the surrogate structural uncertainty by obtaining an ensemble of competing surrogates. In this way, the high-fidelity outputs are likely to be covered by the uncertainty range of the surrogate outputs. Nevertheless, adopting Strategy A will make the approximated posterior wider. In the second strategy (Strategy B), a machine learning method, i.e., Gaussian process, is used to directly simulate the difference between the high-fidelity and the surrogate model outputs. Different from Strategy A, Strategy B generates a directional leap from the surrogate outputs to the corresponding high-fidelity outputs, thus, it introduces less uncertainty. As our concern is the posterior distribution, we propose an active learning process that gradually refines the surrogate in this region. With enough iterations, the surrogate structural error can be reduced to a very low level.

To demonstrate the performance of the proposed approach, we test a numerical case of groundwater contaminant source identification with 28 unknown input variables. It is shown that if the surrogate error is not quantitatively considered in MCMC

simulation, the inversion results will be significantly biased. Without increasing the number of the high-fidelity model evaluations, Strategy A and Strategy B can reduce the bias introduced by the surrogate structural error. In comparing the two strategies, we find that Strategy B has a better performance, as it integrates two methods (i.e., LARS-PCE and GP) that complement each other.

Here, we adopt MCMC to infer the unknown model inputs, the two strategies proposed in this work can also be applied with other inverse algorithms, e.g., ensemble Kalman filter and its variants. Moreover, although the sparse PCE surrogate is utilized in this work, the proposed framework can be also combined with other surrogate modeling techniques for better performances in specific problems. Nevertheless, there are some issues that have not been addressed in this work. For example, we assume the high-fidelity model is perfect. While in practice we should also consider the structural error of the high-fidelity model (i.e., the conceptual model error). In future works, we will simultaneously consider the surrogate and the conceptual model errors by combining the approach proposed in this work with methods proposed in (*Duan et al., 2007; Madadgar & Moradkhani, 2014; Xu & Valocchi, 2015; Xu et al., 2017; Ye et al., 2010*).

Moreover, the two kinds of errors can be reduced in the posterior region in an adaptive manner.

Acknowledgments

Computer codes and data used in this paper are available at:

https://www.researchgate.net/publication/326477215_Adaptive_Surrogate-Based_MCMC_Considering_Surrogate_Structural_Error

This work is supported by the National Natural Science Foundation of China (grants

41771254 and 41571215).

The authors would like to thank Prof. Bruno Sudret from ETH Zurich for providing the UQLab toolbox, Maziar Raissi from Brown University for providing the MATLAB codes of GP, Jasper Vrugt from University of California, Irvine for providing the MATLAB codes of DREAM_(zs), respectively.

References

Ahmad, A., El-Shafie, A., Razali, S. F. M., & Mohamad, Z. S. (2014). Reservoir optimization in water resources: a review. *Water resources management*, 28(11), 3391-3405. <https://doi.org/10.1007/s11269-014-0700-5>

Arnst, M., Ghanem, R., & Soize, C. (2010). Identification of Bayesian posteriors for coefficients of chaos expansions. *Journal of Computational Physics*, 229(9), 3134-3154. <https://doi.org/10.1016/j.jcp.2009.12.033>

Asher, M., Croke, B., Jakeman, A., & Peeters, L. (2015). A review of surrogate models and their application to groundwater modeling. *Water Resources Research*, 51(8), 5957-5973. <https://doi.org/10.1002/2015WR016967>

Blatman, G., & Sudret, B. (2008). Sparse polynomial chaos expansions and adaptive stochastic finite elements using a regression approach. *Comptes Rendus Mécanique*, 336(6), 518-523. <https://doi.org/10.1016/j.crme.2008.02.013>

Blatman, G., & Sudret, B. (2010). Efficient computation of global sensitivity indices using sparse polynomial chaos expansions. *Reliability Engineering & System Safety*, 95(11), 1216-1229. <https://doi.org/10.1016/j.ress.2010.06.015>

Blatman, G., & Sudret, B. (2011). Adaptive sparse polynomial chaos expansion based on least angle regression. *Journal of Computational Physics*, 230(6), 2345-2367. <https://doi.org/10.1016/j.jcp.2010.12.021>

Brooks, S., Gelman, A., Jones, G. L., & Meng, X.-L. (2011). *Handbook of Markov Chain Monte Carlo*. Boca Raton, FL: Chapman & Hall/CRC

Cao, T., Zeng, X., Wu, J., Wang, D., Sun, Y., Zhu, X., Lin, J., & Long, Y. (2018). Integrating MT-DREAMzs and nested sampling algorithms to estimate marginal likelihood and comparison with several other methods. *Journal of Hydrology*, 563, 750-765. <https://doi.org/10.1016/j.jhydrol.2018.06.055>

Chen, Y., & Zhang, D. (2006). Data assimilation for transient flow in geologic formations via ensemble Kalman filter. *Advances in Water Resources*, 29(8), 1107-1122. <https://doi.org/10.1016/j.advwatres.2005.09.007>

Choi, S.-K., Grandhi, R. V., Canfield, R. A., & Pettit, C. L. (2004). Polynomial chaos expansion with latin hypercube sampling for estimating response variability. *AIAA journal*, 42(6), 1191-1198. <https://doi.org/10.2514/1.2220>

Duan, Q., Sorooshian, S., & Gupta, V. (1992). Effective and efficient global optimization for conceptual rainfall-runoff models. *Water Resources Research*, 28(4), 1015-1031. <https://doi.org/10.1029/91WR02985>

Duan, Q., Ajami, N. K., Gao, X., & Sorooshian, S. (2007). Multi-model ensemble hydrologic prediction using Bayesian model averaging. *Advances in Water Resources*, 30(5), 1371-1386. <https://doi.org/10.1016/j.advwatres.2006.11.014>

Efron, B., Hastie, T., Johnstone, I., & Tibshirani, R. (2004). Least angle regression. *The Annals of statistics*, 32(2), 407-499

Elsheikh, A. H., Hoteit, I., & Wheeler, M. F. (2014). Efficient Bayesian inference of subsurface flow models using nested sampling and sparse polynomial chaos surrogates. *Computer Methods in Applied Mechanics and Engineering*, 269, 515-537. <https://doi.org/10.1016/j.cma.2013.11.001>

Emerick, A. A., & Reynolds, A. C. (2013). Ensemble smoother with multiple data assimilation. *Computers & Geosciences*, 55, 3-15. <https://doi.org/10.1016/j.cageo.2012.03.011>

Evensen, G. (2009). *Data assimilation: the ensemble Kalman filter*. Heidelberg, Germany: Springer-Verlag Berlin Heidelberg

Gaume, E., Gaál, L., Viglione, A., Szolgay, J., Kohnová, S., & Blöschl, G. (2010). Bayesian MCMC approach to regional flood frequency analyses involving extraordinary flood events at ungauged sites. *Journal of Hydrology*, 394(1-2), 101-117. <https://doi.org/10.1016/j.jhydrol.2010.01.008>

Goharian, E., Zahmatkesh, Z., & Sandoval-Solis, S. (2018). Uncertainty Propagation of Hydrologic Modeling in Water Supply System Performance: Application of Markov Chain Monte Carlo Method. *Journal of Hydrologic Engineering*, 23(5), 04018013. [https://doi.org/10.1061/\(ASCE\)HE.1943-5584.0001646](https://doi.org/10.1061/(ASCE)HE.1943-5584.0001646)

Gong, W., & Duan, Q. (2017). An adaptive surrogate modeling-based sampling strategy for parameter optimization and distribution estimation (ASMO-PODE). *Environmental Modelling & Software*, 95, 61-75. <https://doi.org/10.1016/j.envsoft.2017.05.005>

Harbaugh, A. W., Banta, E. R., Hill, M. C., & McDonald, M. G. (2000). MODFLOW-2000, The U. S. Geological Survey Modular Ground-Water Model-User Guide to Modularization Concepts and the Ground-Water Flow Process. Reston, VA: U.S. Geological Survey. Retrieved from <https://pubs.usgs.gov/of/2000/0092/report.pdf>

Hastings, W. K. (1970). Monte Carlo sampling methods using Markov chains and their applications. *Biometrika*, 57(1), 97-109

Kuczera, G., Kavetski, D., Renard, B., & Thyer, M. (2010). A limited-memory acceleration strategy for MCMC sampling in hierarchical Bayesian calibration of hydrological models. *Water Resources Research*, 46(7), W07602. <https://doi.org/10.1029/2009WR008985>

Laloy, E., & Vrugt, J. A. (2012). High-dimensional posterior exploration of hydrologic models using multiple-try DREAM (ZS) and high-performance computing. *Water Resources Research*, 48(1), W01526. <https://doi.org/10.1029/2011WR010608>

Laloy, E., Rogiers, B., Vrugt, J. A., Mallants, D., & Jacques, D. (2013). Efficient posterior exploration of a high-dimensional groundwater model from two-stage Markov chain Monte Carlo simulation and polynomial chaos expansion. *Water Resources Research*, 49(5), 2664-2682. <https://doi.org/10.1002/wrcr.20226>

Liu, Y., & Gupta, H. V. (2007). Uncertainty in hydrologic modeling: Toward an integrated data assimilation framework. *Water Resources Research*, 43(7), W07401. <https://doi.org/10.1029/2006WR005756>

Madadgar, S., & Moradkhani, H. (2014). Improved Bayesian multimodeling: Integration of copulas and Bayesian model averaging. *Water Resources Research*, 50(12), 9586-9603. <https://doi.org/10.1002/2014WR015965>

Marelli, S., & Sudret, B. (2014). UQLab: A framework for uncertainty quantification in Matlab, paper presented at Second International Conference on Vulnerability and Risk Analysis and Management (ICVRAM), Liverpool, United Kingdom. <https://doi.org/10.1061/9780784413609.257>

Metropolis, N., Rosenbluth, A. W., Rosenbluth, M. N., Teller, A. H., & Teller, E. (1953). Equation of state calculations by fast computing machines. *The journal of chemical physics*, 21(6), 1087-1092. <https://doi.org/10.1063/1.1699114>

Moradkhani, H., Hsu, K. L., Gupta, H., & Sorooshian, S. (2005). Uncertainty assessment of hydrologic model states and parameters: Sequential data assimilation using the particle filter. *Water Resources Research*, 41(5), W05012. <https://doi.org/10.1029/2004WR003604>

Osorio-Murillo, C. A., Over, M. W., Savoy, H., Ames, D. P., & Rubin, Y. (2015). Software framework for inverse modeling and uncertainty characterization. *Environmental Modelling & Software*, 66, 98-109.

<https://doi.org/10.1016/j.envsoft.2015.01.002>

Rasmussen, C. E., & Williams, C. K. (2006). *Gaussian Process for Machine Learning*. Cambridge, MA: the MIT press

Razavi, S., Tolson, B. A., & Burn, D. H. (2012). Review of surrogate modeling in water resources. *Water Resources Research*, 48(7), W07401. <https://doi.org/10.1029/2011WR011527>

Reed, P. M., Hadka, D., Herman, J. D., Kasprzyk, J. R., & Kollat, J. B. (2013). Evolutionary multiobjective optimization in water resources: The past, present, and future. *Advances in Water Resources*, 51, 438-456. <https://doi.org/10.1016/j.advwatres.2012.01.005>

Schoups, G., & Vrugt, J. A. (2010). A formal likelihood function for parameter and predictive inference of hydrologic models with correlated, heteroscedastic, and non-Gaussian errors. *Water Resources Research*, 46(10), W10531. <https://doi.org/10.1029/2009WR008933>

Smith, R. C. (2014). *Uncertainty Quantification: Theory, Implementation, and Applications*. Philadelphia, Pa.: SIAM

Smith, T. J., & Marshall, L. A. (2008). Bayesian methods in hydrologic modeling: A study of recent advancements in Markov chain Monte Carlo techniques. *Water Resources Research*, 44(12), W00B05. <https://doi.org/10.1029/2007WR006705>

Song, X., Shi, L., Ye, M., Yang, J., & Navon, I. M. (2014). Numerical comparison of iterative ensemble Kalman filters for unsaturated flow inverse modeling. *Vadose Zone Journal*, 13(2). <https://doi.org/10.2136/vzj2013.05.0083>

Song, X., Zhang, J., Zhan, C., Xuan, Y., Ye, M., & Xu, C. (2015). Global sensitivity analysis in hydrological modeling: Review of concepts, methods, theoretical framework, and applications. *Journal of Hydrology*, 523, 739-757. <https://doi.org/10.1016/j.jhydrol.2015.02.013>

Tartakovsky, D. M. (2013). Assessment and management of risk in subsurface hydrology: A review and perspective. *Advances in Water Resources*, 51, 247-260. <https://doi.org/10.1016/j.advwatres.2012.04.007>

Vrugt, J. A. (2016). Markov chain Monte Carlo simulation using the DREAM software package: Theory, concepts, and MATLAB implementation. *Environmental Modelling & Software*, 75, 273-316. <https://doi.org/10.1016/j.envsoft.2015.08.013>

Vrugt, J. A., & Beven, K. J. (2018). Embracing equifinality with efficiency: Limits of Acceptability sampling using the DREAM(LOA) algorithm. *Journal of Hydrology*, 559, 954-971. <https://doi.org/10.1016/j.jhydrol.2018.02.026>

Vrugt, J. A., Gupta, H. V., Bouten, W., & Sorooshian, S. (2003). A Shuffled Complex Evolution Metropolis algorithm for optimization and uncertainty assessment of hydrologic model parameters. *Water Resources Research*, 39(8), 1201. <https://doi.org/10.1029/2002WR001642>

Vrugt, J. A., ter Braak, C. J., Diks, C. G., & Schoups, G. (2013). Hydrologic data assimilation using particle Markov chain Monte Carlo simulation: Theory, concepts and applications. *Advances in Water Resources*, 51, 457-478. <https://doi.org/10.1016/j.advwatres.2012.04.002>

Vrugt, J. A., Ter Braak, C. J., Clark, M. P., Hyman, J. M., & Robinson, B. A. (2008). Treatment of input uncertainty in hydrologic modeling: Doing hydrology backward with Markov chain Monte Carlo simulation. *Water Resources Research*, 44(12), W00B09. <https://doi.org/10.1029/2007WR006720>

Weerts, A. H., & El Serafy, G. Y. (2006). Particle filtering and ensemble Kalman filtering for state updating with hydrological conceptual rainfall-runoff models. *Water Resources Research*, 42(9), W09403. <https://doi.org/10.1029/2005WR004093>

Xiu, D. (2010). *Numerical methods for stochastic computations: a spectral method approach*. Princeton,

NJ: Princeton University Press

Xu, T., & Valocchi, A. J. (2015). A Bayesian approach to improved calibration and prediction of groundwater models with structural error. *Water Resources Research*, 51(11), 9290-9311. <https://doi.org/10.1002/2015WR017912>

Xu, T., Valocchi, A. J., Ye, M., & Liang, F. (2017). Quantifying model structural error: Efficient Bayesian calibration of a regional groundwater flow model using surrogates and a data - driven error model. *Water Resources Research*, 53(5), 4084-4105. <https://doi.org/10.1002/2016WR019831>

Ye, M., Pohlmann, K. F., Chapman, J. B., Pohll, G. M., & Reeves, D. M. (2010). A model-averaging method for assessing groundwater conceptual model uncertainty. *Groundwater*, 48(5), 716-728. <https://doi.org/10.1111/j.1745-6584.2009.00633.x>

Zeng, L., Shi, L., Zhang, D., & Wu, L. (2012). A sparse grid based Bayesian method for contaminant source identification. *Advances in Water Resources*, 37, 1-9. <https://doi.org/10.1016/j.advwatres.2011.09.011>

Zhang, D., & Lu, Z. (2004). An efficient, high-order perturbation approach for flow in random porous media via Karhunen-Loèvè and polynomial expansions. *Journal of Computational Physics*, 194(2), 773-794. <https://doi.org/10.1016/j.jcp.2003.09.015>

Zhang, G., Lu, D., Ye, M., Gunzburger, M., & Webster, C. (2013). An adaptive sparse-grid high-order stochastic collocation method for Bayesian inference in groundwater reactive transport modeling. *Water Resources Research*, 49(10), 6871-6892. <https://doi.org/10.1002/wrcr.20467>

Zhang, J., Li, W., Zeng, L., & Wu, L. (2016). An adaptive Gaussian process-based method for efficient Bayesian experimental design in groundwater contaminant source identification problems. *Water Resources Research*, 52(8), 5971-5984. <https://doi.org/10.1002/2016WR018598>

Zhang, J., Zeng, L., Chen, C., Chen, D., & Wu, L. (2015). Efficient Bayesian experimental design for contaminant source identification. *Water Resources Research*, 51(1), 576-598. <https://doi.org/10.1002/2014WR015740>

Zhang, J., Li, W., Lin, G., Zeng, L., & Wu, L. (2017). Efficient evaluation of small failure probability in high-dimensional groundwater contaminant transport modeling via a two-stage Monte Carlo method. *Water Resources Research*, 53(3), 1948-1962. <https://doi.org/10.1002/2016WR019518>

Zhang, J., Man, J., Lin, G., Wu, L., & Zeng, L. (2018a). Inverse modeling of hydrologic systems with adaptive multi-fidelity Markov chain Monte Carlo simulations. *Water Resources Research*, In Press. <https://doi.org/10.1029/2018WR022658>

Zhang, J., Lin, G., Li, W., Wu, L., & Zeng, L. (2018b). An iterative local updating ensemble smoother for estimation and uncertainty assessment of hydrologic model parameters with multimodal distributions. *Water Resources Research*, 54(3), 1716-1733. <https://doi.org/10.1002/2017WR020906>

Zheng, C., & Wang, P. P. (1999). MT3DMS: a modular three-dimensional multispecies transport model for simulation of advection, dispersion, and chemical reactions of contaminants in groundwater systems; documentation and user's guide: DTIC Document. Retrieved from <http://www.geology.wisc.edu/courses/g727/mt3dmanual.pdf>

Table

Table 1 Prior ranges and true values of the contaminant source parameters

Parameter	Range	True value
x_s [L]	[3-5]	4.033
y_s [L]	[4-6]	5.405
s_1 [MT $^{-1}$]	[0-8]	1.229
s_2 [MT $^{-1}$]	[0-8]	7.628
s_3 [MT $^{-1}$]	[0-8]	4.327
s_4 [MT $^{-1}$]	[0-8]	5.438
s_5 [MT $^{-1}$]	[0-8]	0.293
s_6 [MT $^{-1}$]	[0-8]	6.474

Figures

Figure 1. Flow domain of the numerical case.

Figure 2. Trace plots of the high-fidelity MCMC (blue dots), posterior mean estimates obtained from $\hat{f}(\mathbf{m})$ -MCMC (red circles), $\hat{f}(\mathbf{m})$ -MCMC+Strategy A (red diamonds), and $\hat{f}(\mathbf{m})$ -MCMC+Strategy B (red squares), respectively. Here the eight panels are for the eight contaminant source parameters, and the true values are represented by the black crosses.

Figure 3. Initial and added training data generated in the $\hat{f}(\mathbf{m})$ -MCMC approach. Here the eight panels are for the eight contaminant source parameters, and the true values are represented by the black crosses.

Figure 4. Initial and added training data generated in the $\hat{f}(\mathbf{m})$ -MCMC+Strategy A approach. Here the eight panels are for the eight contaminant source parameters, and the true values are represented by the black crosses.

Figure 5. Initial and added training data generated in the $\hat{f}(\mathbf{m})$ -MCMC+Strategy B approach. Here the eight panels are for the eight contaminant source parameters, and the true values are represented by the black crosses.

Figure 6. Evolution of the error of the LARS-PCE surrogate at the true model parameters. Here the error index at the y axis is calculated with equation (19).

No flow

10 [L]

Measurement locations

$h = 12$ [L]

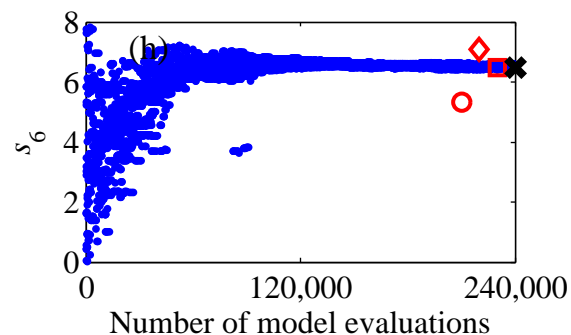
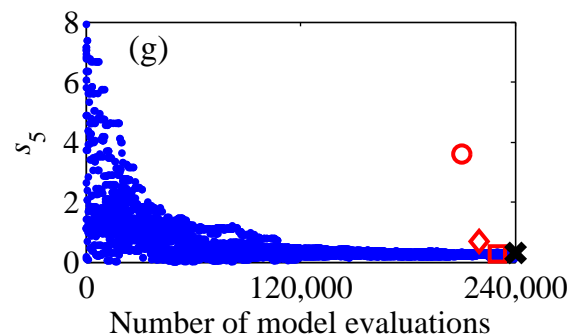
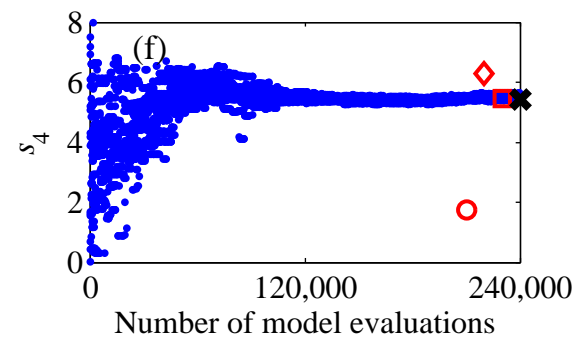
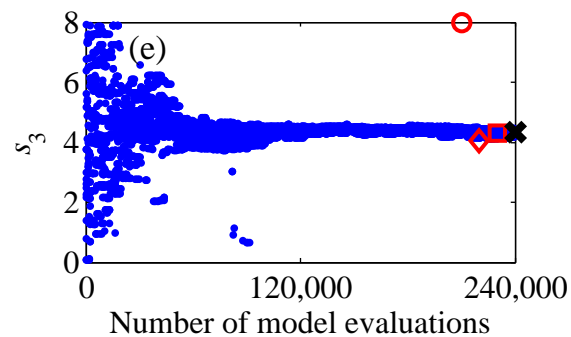
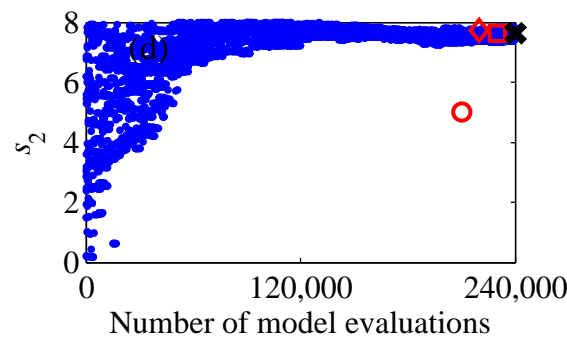
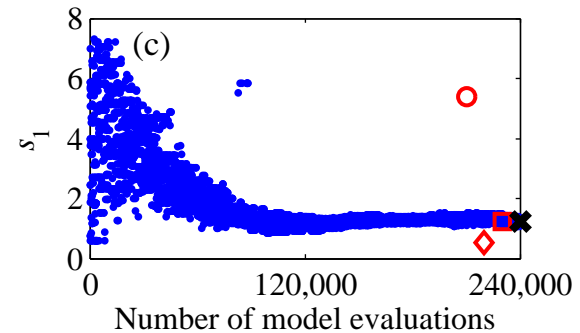
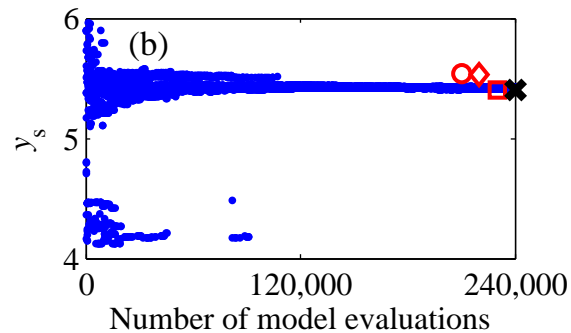
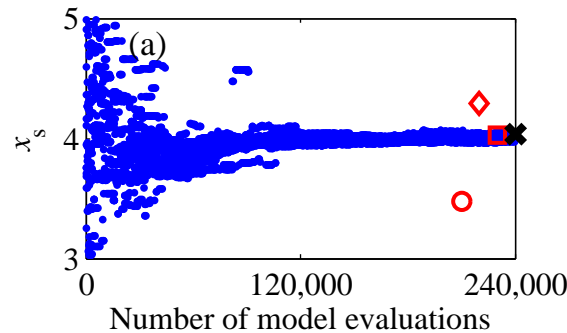
$h = 11$ [L]

s

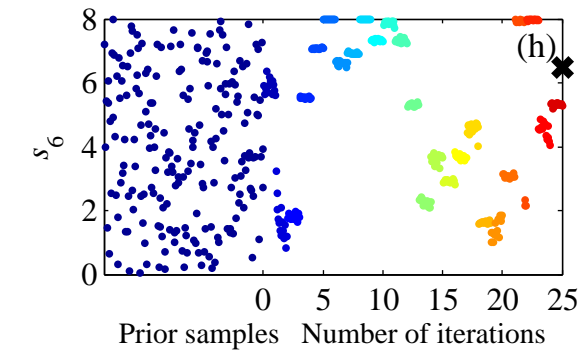
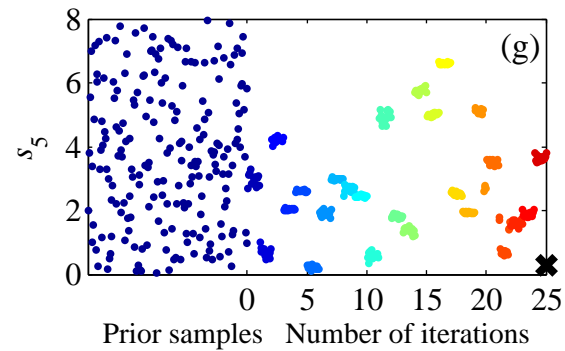
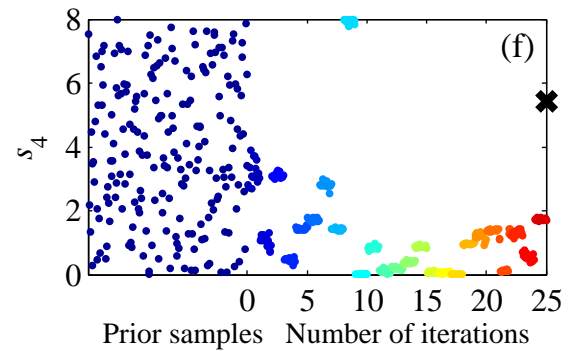
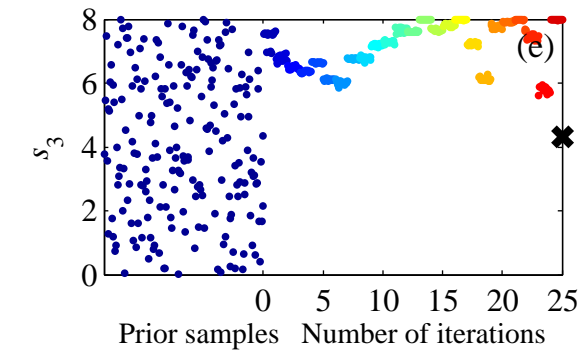
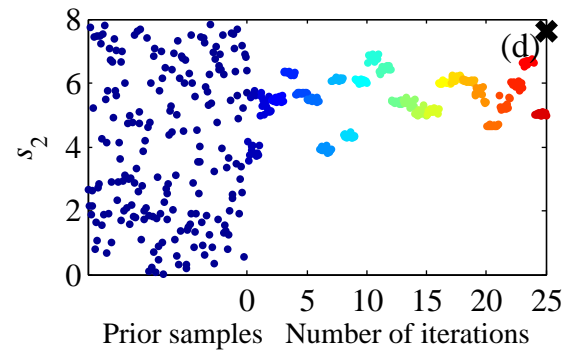
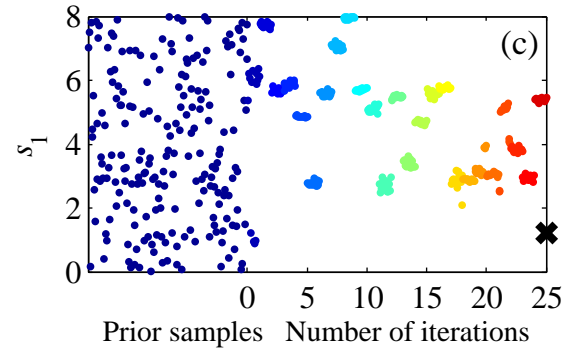
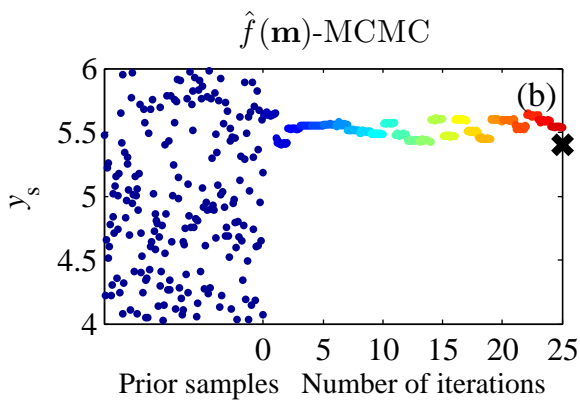
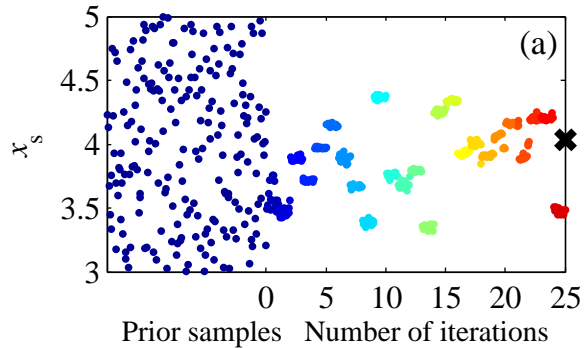
0

20 [L]

No flow

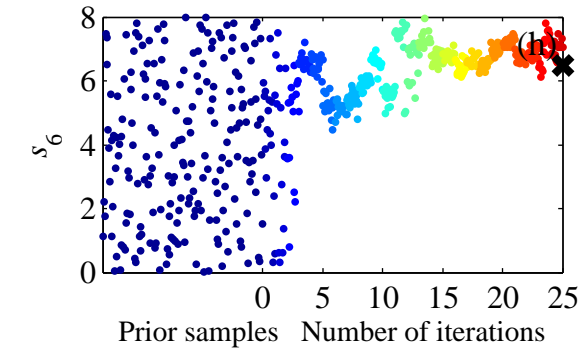
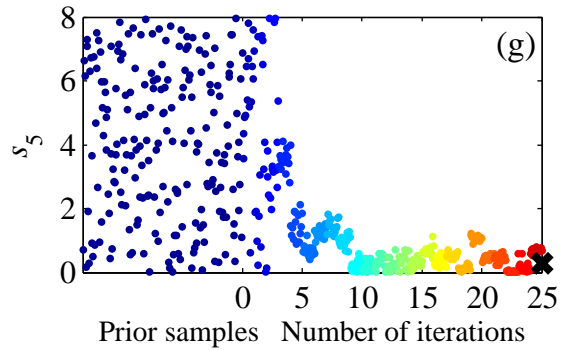
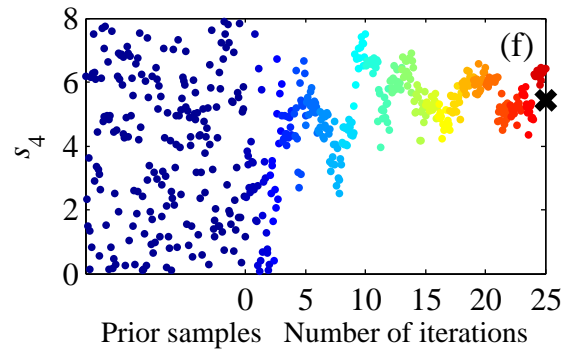
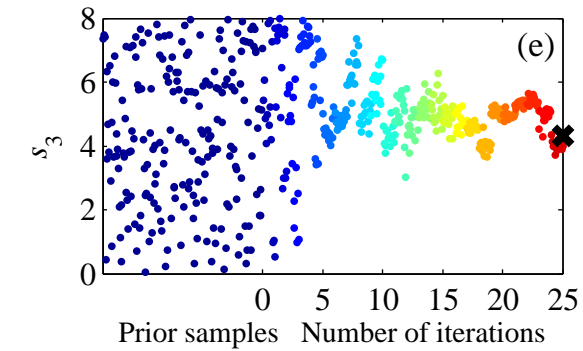
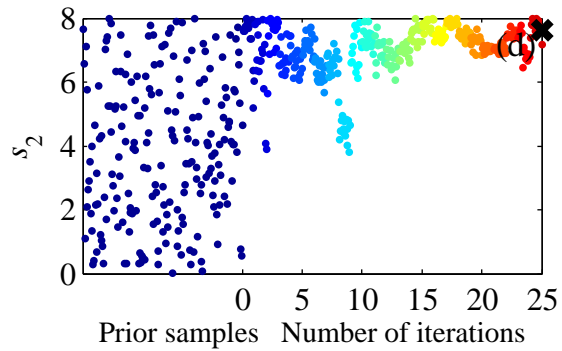
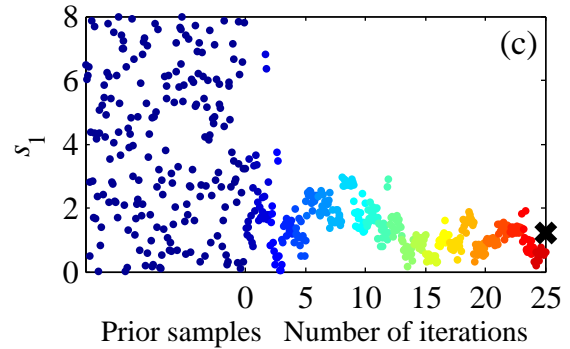
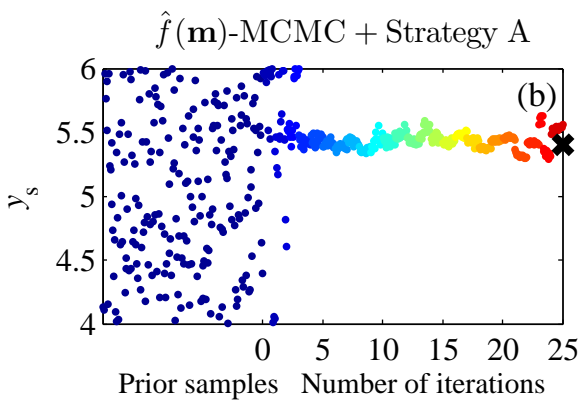
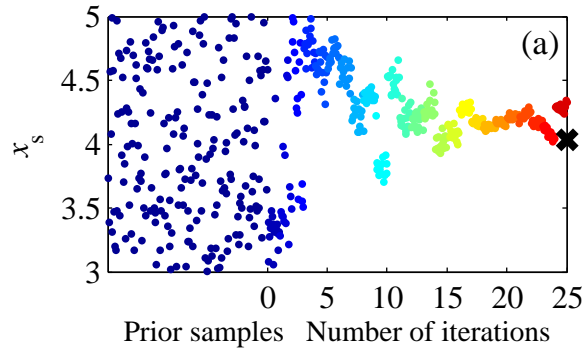


- Reference results
- $\hat{f}(\mathbf{m})$ -MCMC
- ◊ $\hat{f}(\mathbf{m})$ -MCMC + Strategy A
- ◻ $\hat{f}(\mathbf{m})$ -MCMC + Strategy B
- ✖ True value



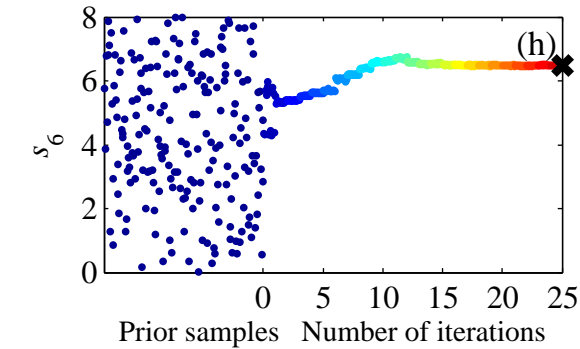
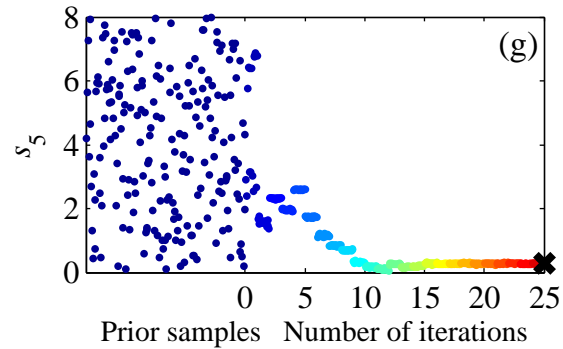
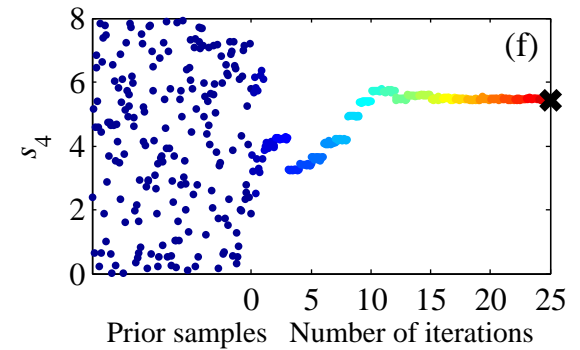
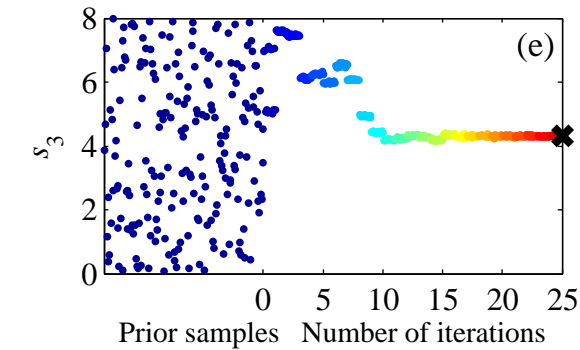
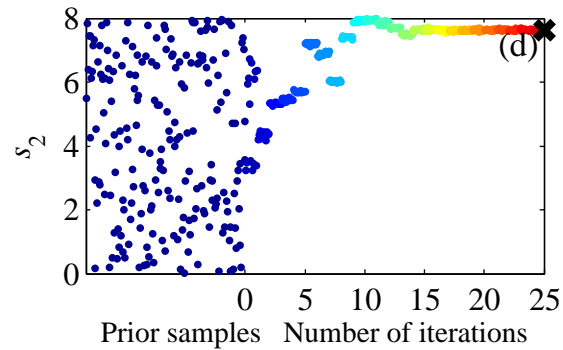
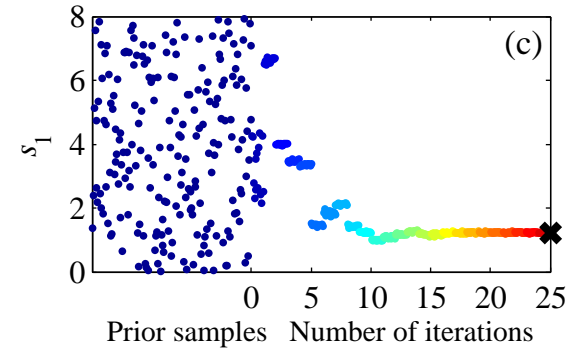
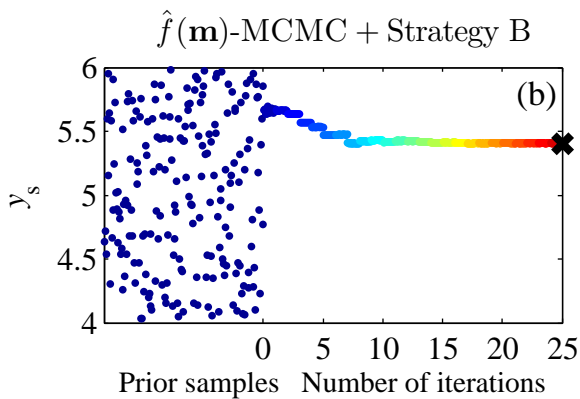
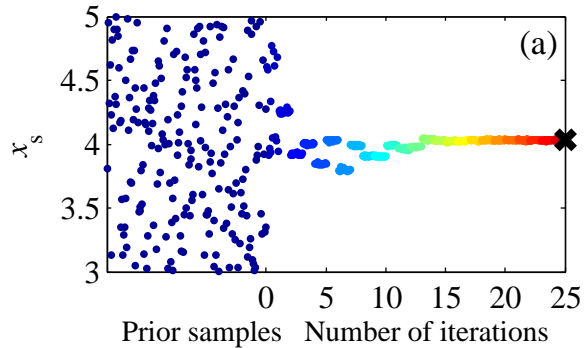
True value

Number of $f(\mathbf{m})$ evaluations : 700



True value

Number of $f(\mathbf{m})$ evaluations : 700



True value

Number of $f(\mathbf{m})$ evaluations : 700

